



Design and development of a novel fixed-wing biplane micro air vehicle with enhanced static stability

Shuvrangshu Jana¹ · Harikumar Kandath¹ · Mayur Shewale¹ · Gunjit Dhingra¹ · Duddela Sai Harish¹ · M. Seetharama Bhat¹

Received: 16 June 2021 / Revised: 4 December 2021 / Accepted: 13 January 2022 / Published online: 10 February 2022
© Deutsches Zentrum für Luft- und Raumfahrt e.V. 2022

Abstract

A detailed design approach undertaken in the development of “Skylark” is presented in this paper. “Skylark” is a non-conventional fixed-wing biplane Micro Air Vehicle (MAV) with a wingspan and chord length within 150 mm. It is specially designed with the ability to host onboard vision-assisted autonomous navigation systems. Fixed-wing MAV with capabilities of vision assisted autonomous navigation is not reported in the open literature. To stay within the maximum dimensional constraint, flying wing configuration with a low aspect ratio is preferred for MAV design, and therefore, the stability is inadequate due to lower static margin when compared to bigger Unmanned Aerial Vehicles (UAVs). In this paper, the novel design strategy addresses the major challenges such as high payload-carrying capacity, stability, and onboard processing required for vision-assisted autonomous navigation. The higher payload-carrying capacity is addressed by considering biplane aerodynamic configuration, while the longitudinal static margin is improved by placing the top lifting surface toward the trailing edge. A powerful yet compact and lightweight autopilot is designed to perform image processing algorithms onboard. Detailed design is done based on the requirement of the centre of gravity location by suitable weight distribution. The stability of the designed biplane is validated through several flight tests. The proposed novel design methodology of adding optimal top plane provides flexibility in managing static margin based on mission profile compared to monoplane MAVs.

Keywords Biplane · Micro air vehicle · Fixed wing · Stability · Vehicle design · Flying wing

List of symbols

α_a	Absolute angle of attack of whole body	$C_{M, cg}$	Pitching moment coefficient about centre of gravity
α_{w1} , and $\alpha_{w1} - \epsilon$	Absolute angle of attack of the bottom wing and top wing, respectively	C_{l_p}	Slope of the rolling moment coefficient vs side slip angle
ac_v	Aerodynamic centre of vertical tail	C_{n_p}	Slope of the yawing moment coefficient vs side slip angle
a_{w1} , a_{w2}	Slope of the lift curve of bottom wing and top wing	D_{w1} , D_{w2}	Drag forces acting on top and bottom wing
c	Mean zero lift chord of bottom wing	e	Span efficiency factor
C_D	Total drag coefficient	ϵ	Downwash angle
C_{D_e}	Profile drag coefficient	G_1	Vertical distance between zero lift chord line of the top wing and bottom wing
C_L	Lift force coefficient	h , $h_{ac_{w1}}$	Distance of CG and aerodynamic centre of the whole configuration from the leading edge of the bottom wing in a fraction of chord length of the bottom wing
C_m	Pitching moment coefficient		
$C_{M,0}$	Moment coefficient about the centre of gravity at zero lift		
C_{m_α}	Slope of pitching moment coefficient vs angle of attack	k	Chord length of the top wing in the fraction of chord length of the bottom wing

✉ Shuvrangshu Jana
shuvra.ce@gmail.com

¹ Indian Institute of Science, Bangalore, India

l_{w2}	Horizontal distance of the aerodynamic centre of the top wing from the centre of gravity of the MAV
L_{w1}, L_{w2}	Lift and drag forces acting on top and bottom wing
L_3	Distance between the aerodynamic centre of the top wing and bottom wing
L_2	horizontal distance of the mean aerodynamic centre from the bottom wing's aerodynamic centre
M_{cgw1}	Moment of the bottom wing about the centre of gravity of MAV
M_{cgw2}	Moment of the top wing about the centre of gravity of MAV
$M_{ac,w1}, M_{ac,w2}$	The moment of the top and bottom wing about their aerodynamic centre
μ	Angle between the bottom chord and line joining the aerodynamic centre of the top wing and bottom wing
q_∞	Dynamic pressure
S_w	Reference surface area of wing
S_{w2}	Reference surface area of bottom wing
S_{w1}	Reference surface area of top wing
W_H	Wing volume ratio
x	The horizontal distance of the centre of gravity from the bottom wing's aerodynamic centre
z_{w1}	The vertical distance of the centre of gravity from the mean zero lift chord of the bottom wing in a fraction of bottom chord length
z_{cg}	The vertical distance of the centre of gravity from the mean zero lift chord of the bottom wing

Acronyms

AR	Aspect ratio
CG	Centre of gravity
MAV	Micro air vehicle
RC	Remote controlled
UAV	Unmanned aerial vehicle

1 Introduction

Micro air vehicles (MAVs) are attracting increasing attention in civil and military applications as they have the capability to perform critical tasks that may pose a threat to human lives, such as surveying in a hazardous environment. MAV was originally defined as an aerial vehicle having a maximum dimension of 150 mm or less and velocity around 10–20 m/s [1]. Owing to the aerodynamic advantage, the fixed-wing MAVs are a better choice as opposed to other

types of MAVs when the mission requires higher speed, longer endurance, and higher payload-carrying capacity. Furthermore, fixed-wing MAVs are also operationally silent. Numerous fixed-wing MAVs of different configurations, possessing capability of remote-controlled or semi-autonomous flight are reported in the open literature, for example, Black Widow [2], SPOT [3], UGMV15 [4], KH2013A [5], etc. Hereafter, fixed-wing MAV is denoted as MAV.

“Black Widow,” developed by Aerovironment Inc. USA as a part of the DARPA project, is widely considered as the first generation of successful MAV. It has a wingspan of 6 inches, a total mass of 80 g, an endurance of 30 min. The velocity of the “Black Widow” has been reported around 25 mph (11.17 m/s). Its autopilot is capable of altitude hold, airspeed hold, heading hold. The autonomous waypoint navigation capability of this vehicle is not reported in the literature. “SP OT” MAV is designed with a wingspan of 15 cm, a total mass of 75 g, and an endurance of 2 min. It is reported that low endurance is due to the lack of stability. Provision of autopilot hardware is not mentioned. “KH2013A” is designed with a total mass of 53 g, with a velocity range of 6–13 m/s and an endurance of 4 min. “UGMAV15” is designed using design optimization with a primary objective of maximum endurance with a total mass of 58 g; however, only a preliminary flight test is reported. Some of the important challenges associated with the MAV design are reduction of maximum lift-to-drag ratio due to formation of laminar separation bubble [6], dynamic coupling [5], high sensitivity to rolling and pitching moments due to low inertia, low static margin, low bandwidth actuator, sensitive to wind gust due to velocity comparable with wind velocity, etc. Mathematical modelling of MAV is reported in the literature using first principle modelling [7] and system identification approach [8]. In the first principle methods, the system parameter is obtained using the basic aircraft mechanics, software like XFLR/ CAD, and wind tunnel test. On the other hand, in the system identification method, parameters are developed from flight test results.

In line with the current trend, the next generation of MAVs needs to possess capabilities, such as performing autonomous waypoint navigation in a GPS-denied environment, surveying the target area while having the real-time intelligence to adjust the mission in an unknown and obstacle prone environment. Furthermore, integrating cameras in an MAV system makes it possible to compute the state information of the MAV in addition to obstacle detection and avoidance while simultaneously providing surveillance footage, thus making way for the next generation of navigation systems.

To accommodate all the design requirements, non-conventional designs need to be explored. Different types of non-conventional configurations are reported in the literature to achieve a specific performance criterion such as a better

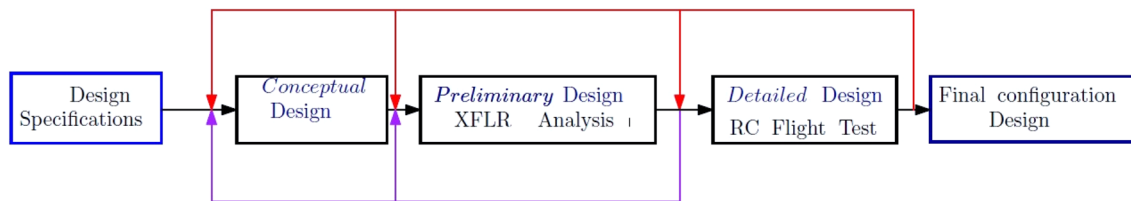


Fig. 1 Design flowchart

aerodynamic efficiency or a high payload-carrying capacity, etc. [9–20]. “TYTO”, a low-speed biplane, is designed with a total weight of 100 g and with a wingspan of 30 cm [9]. Biplane with inverse Zimmerman planform is proposed in [11], where the top wing is kept forward than the bottom wing; however, flight tests are not reported. A tailless biplane configuration, “XPlane”, having a wingspan of 40 cm and a total weight of 400 g, is conceptually proposed to increase the payload capacity while retaining the system stability and controllability characteristics [16]. In [12], design and testing of 1:5 scaled model of PrandtlPlane configuration, which is a box wing with two swept lifting wings, are reported, and the advantages of two wings such as improved stability in the lateral and longitudinal direction, the low stall speed is validated through flight tests. However, for the MAV class of vehicles, a non-conventional configuration is not reported in the literature.

In this paper, a novel non-conventional biplane configuration with an optimum top wing at the trailing edge is proposed to meet the primary design requirement of high payload-carrying capacity and good longitudinal static margin. The top plane acts as an additional lifting surface as well as shifts the neutral point of the overall system toward the trailing edge. CG has been maintained ahead of the neutral point by employing multiple strategies such as the placement of the top wing, miniaturized component design, and providing a suitable motor thrust axis. The counter-torque is balanced by placing the vertical tail in the propeller wash and making the asymmetric weight distribution about the forward axis of the MAV. The designed MAV is flight tested in an outdoor environment, and results are presented validating the stability aspects mentioned. Such detailed outdoor flight test results are not reported in the literature for the 150 mm class of biplanes.

An iterative design methodology is used to reach a preliminary configuration via four distinct stages, namely conceptual design stage, preliminary design stage, detailed design stage, and the final configuration is obtained after incorporating the observations from the remote-controlled flight tests. A typical flowchart for MAV design steps is shown in Fig. 1.

A similar design approach is followed in the case of conventional bigger aircraft design [21], but in this case, flight

test observations are incorporated in finalizing the aerodynamics configuration and avionics selection.

The main contributions of the paper are the following aspects:

- Novel non-conventional aerodynamic configuration design for heavier payload and better static margin.
- Development of the various subsystem of MAV having capabilities of vision-assisted autonomous navigation.

The rest of the paper is described as follows. Important design specifications and design challenges are discussed in Sect. 2. Based on the design specifications, a conceptual MAV configuration is proposed, and its realizability is examined in the conceptual design stage in Sect. 3. Section 4 describes the preliminary design of the wing, tail, control surface, and analysis of the configuration in XFLR software. Detailed design of the propulsion system, avionics, and structure are performed in Sect. 5. Section 6 presents the final configuration of “Skylark” and flight test results.

2 Design requirement and challenges

A typical mission profile of MAV comprises reaching the designated area quickly within a distance of approximately 1.5 km, slowly loitering, say, thrice over the objective zone in a circle with a diameter of 50 m. The mission requires capturing and processing images to assist MAV state estimation, obstacle detection, and avoidance, etc., and finally return to the launch location. This mission profile of MAV is for a typical application of MAVs, such as in the front line area of a warzone where MAV needs to go to the enemy zone and capture the images and get back to home location.

MAV having the capabilities mentioned above must incorporate the main autopilot for low-level real-time tasks such as attitude estimation and stabilization, an image processing module, vision sensors, battery, motor, electronic speed controller, receiver, GPS, and a telemetry module. The maximum velocity needs to be kept within a specific limit to capture better quality images through a lightweight camera; therefore, for the current design, the nominal velocity is selected as 10 m/s, which is also a typical maximum

Table 1 Approximate weight breakup

Component	Weight (g)
Autopilot	15
Battery	20
Servos	4
Motor and propeller	10
Electronic speed controller	6
Camera	5
Payload	10
Structure	30
Miscellaneous	10

speed of conventional MAVs [2–5]. It is desirable that the longitudinal stability margin is kept at least 5–8% for the safe and reliable mission [22]. However, a higher stability margin of about 8–12% is preferable for more reliability, because the allowable range of CG variation in MAVs is less compared to bigger planes.

The total distance to be covered by the MAV is approximately 4 km for a typical mission profile as the one specified above. Therefore, in a no-wind condition, an endurance of 7–8 min is required to complete the mission profile. It is assumed that the effect of wind on total endurance will be small for a to and fro mission.

There is no design standard available in the open literature that specifically addresses the flying qualities for the small-scale vehicles [23]. The natural modes of extremely lightweight low Reynolds numbers are higher than the conventional aircraft [24]. Therefore, the flying qualities standard for the conventional aircraft needs to be modified for application to small-scale platforms [25]. In this case, the flying qualities' requirement of the piloted aircraft as per U.S. military standard such as MIL-STD-1797 [26] and MIL-F-8785C [27] is adopted for the design with a suitable assessment on the flying qualities requirement for MAVs. It is desired that the design must guarantee the level of acceptability to be one in terms of flight and flight safety; that is, “*the flying qualities clearly adequate for mission flight phase*”.

As it is difficult to achieve perfect landing of MAVs all the time, the integrity of the MAV structure needs to be robust to sustain the intermittent bad landing. A preliminary weight estimate of the different components is given in Table 1 based on the required endurance, available hardware, structural materials, and also from the previous experiences of building several small-scale vehicles. Considering all the above aspects, an approximate design specification is presented in Table 2.

In achieving the above design requirements, these are some key design challenges.

Table 2 Preliminary MAV design parameters

Parameter	Specification
Take-off weight	110 g
Expected payload	10 g
Wing span	150 mm
Nominal flight speed	10 m/s
Flight duration	7–8 min
Range	1.5 km
Capability	Vision assisted autonomous navigation
Stability margin	8–12%

- *Total take-off weight* According to Table 1, the design take-off weight is about 110 g. This design prerequisite is high as compared to the maximum reported take-off weight of 80 g among the current flying MAVs [2]. Therefore, enhancing the payload-carrying capacity turns out to be a crucial criterion in MAV system design.
- *Longitudinal stability margin* Generally, a tailless flying wing configuration is preferred to meet the maximum dimension constraint of the MAV. Therefore, MAV has a less static margin and inadequate longitudinal stability. However, as this class of vehicles is sensitive to gusts, the static margin should be higher for a safe and reliable mission. Subsequently, the improvement of static margin is considered as one of the important design criteria. In general, the stability of this class of vehicles needs to be improved.
- *High counter-torque* Propeller rotation induces significant counter-torque, and it severely affects the lateral dynamics of MAV because of its low moment of inertia compared to bigger UAVs. Also, it is difficult to balance the counter-torque with the available control authority.

To address the above challenges, the MAV system design is performed in four stages; conceptual design, preliminary design, detailed component design, and final design. Each of the stages is explained in detail in the following sections.

3 Conceptual design

The basic configuration is developed considering the following important perspectives.

3.1 Increasing the payload capacity

It is hard to accomplish the design requirements in the current scenario, more specifically, the total take-off weight with existing airfoils for the flying wing configuration. High camber airfoil can generate enough lift for the designed

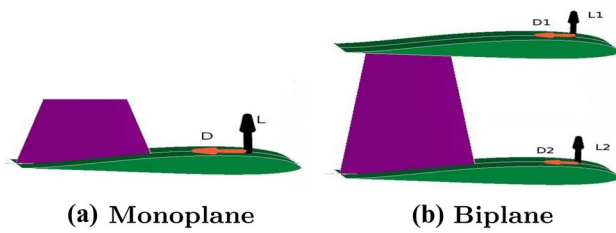


Fig. 2 Comparison between monoplane and biplane

take-off weight; however, it is challenging to balance their high negative pitching moment. In addition, balancing the pitching moment with the propulsive forces for the entire flight duration is unrealistic as propulsive forces vary with battery characteristics.

The idea of increasing the payload-carrying capacity by increasing the velocity of MAV may not work, since an increase in the velocity would have a cascading effect on the weight of other components such as the battery, electronic speed controller, etc., thereby increasing the overall take-off weight. The increase in velocity would also increase drag and counter-torque produced due to the motor, which may not be easy to balance while considering other design constraints. MAV is largely made up of lightweight materials, making it susceptible to vibration due to the motor and propeller combination. This vibration is picked up by sensors, and hence, makes state estimation difficult.

As per the great flight diagram [28], statistically, the approximate wing loading required for the total weight of 110 g is 35, i.e., $W/S = 35$; where W is the weight of total MAV in Newton and S is the surface area in m^2 . Therefore, the approximate wing area required for this wing loading is 315 cm^2 . The maximum area possible for a monoplane wing with a 15 cm span and 15 cm chord is 225 cm^2 . Hence, non-conventional design with the incorporation of additional lifting surfaces needs to be explored. Biplane configuration is more common among non-conventional configurations. When the span is constrained, the biplane configuration can provide better efficiency in terms of high lift and less induced drag than the monoplane. Apart from high payload-carrying capacity biplane will have advantages of low induced drag, low stall speed, and high manoeuvrability [29–35].

Let us consider the effect on aerodynamic efficiency due to the addition of another similar lifting surface on top of the bottom wing, as shown in Fig. 2.

Total drag coefficient (C_D) is the summation of profile drag coefficient (C_{D_e}) and induced drag coefficient, $C_D = C_{D_e} + KC_L^2$; where $K = \frac{1}{\pi e AR}$, C_L is lift force coefficient, e is span efficiency factor, and AR is aspect ratio. The aeroplane aerodynamic efficiency is generally considered in terms of lift-to-drag ratio. For a monoplane configurations,

Table 3 Comparison between monoplane and biplane

Parameter	Monoplane	Biplane
Lift force	$C_L q_\infty S_w$	$2 \times (0.7 C_L) q_\infty S_w$
Drag force	$(C_{D_e} + KC_L^2) q_\infty S_w$	$2 \times (C_{D_e} + 0.49 KC_L^2) q_\infty S_w$
Lift to drag ratio	$\frac{C_L}{C_D}$	$1.0086 \frac{C_L}{C_D}$

the ratio of lift (L) to drag (D) force is $\frac{C_L}{C_D}$. If one similar top wing is added above the bottom wing, the lift coefficient of each wing will be reduced due to interference between the top and bottom wings. Considering a 30% decrease in the lift in each plane, the lift forces (L_1, L_2) will be $0.7 C_L q_\infty S_w$ for each wing and the drag forces (D_1, D_2) will be $(C_{D_e} + K(0.7 C_L)^2) q_\infty S_w$. Here, q_∞ is dynamic pressure and S_w is the reference surface area of the wing. If the extra profile drag of structural support to carry the top plane is small, the ratio of lift-to-drag force of the overall system can be approximated as $\frac{1.4 C_L}{2 C_{D_e} + 0.98 K C_L^2}$.

In general, for the monoplane MAVs, the induced drag is around 60–70% of total drag. Considering induced drag to be 60% of total drag

$$KC_L^2 = 0.6 C_D \quad C_{D_e} = 0.4 C_D.$$

Hence, the lift-to-drag ratio in the case of biplane configuration is $1.0086 \frac{C_L}{C_D}$. Summary of the comparison between monoplane and biplane is shown in Table 3.

Therefore, with biplane configuration and by keeping the profile drag of the extra supporting vertical structures for top wing small, approximately 40% additional lift can be obtained with a similar lift-to-drag ratio. Also, some part of extra lift forces will be required to balance the additional weight of the top wing and vertical supporting structures. Therefore, the effect of the addition of a top wing can make a favourable contribution to the system by considering the following aspects of design:

- Make the top plane and vertical structural support lighter.
- Reduce the profile drag of structural support.
- Maintain an optimum gap between two wings considering the trade-off of the effect of interference on lift force with extra drag and the structural load of vertical support.

As the total lift force required for this design is higher than the existing MAVs, the increment of total load-carrying capacity is considered the main design objective.

3.2 Increasing longitudinal static margin

The distance between the centre of gravity and the neutral point is the measure of the longitudinal stability of the

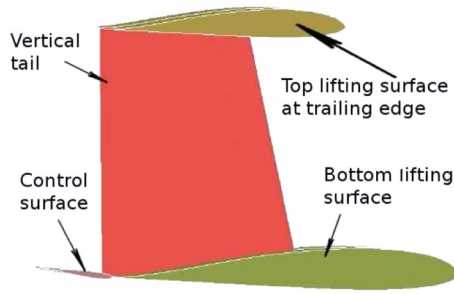


Fig. 3 Conceptual model

aircraft. It is desirable to adjust the centre of gravity toward the forward direction to achieve a higher static stability margin. For the flying wing design, the neutral point of MAVs lies very close to the aerodynamic centre of the wing. As the aerodynamic centre lies nearly 25% of the chord length, the centre of gravity needs to be adjusted within 25% of the chord length.

The extent of bringing the CG nearer to the leading edge is limited by the size of the components and the space required by them. Hence, the longitudinal static margin cannot be improved by a large amount. Instead of the traditional way of adjusting the CG location, the neutral point of the vehicle can be brought toward the trailing edge by including an additional lifting surface near the trailing edge, which will permit a better admissible range of the CG location.

Therefore, lifting surfaces at the trailing edge need to be incorporated to increase the amount of lift as well as to increase the stability margin. A conceptual aerodynamic configuration of MAV, shown in Fig. 3, is proposed to meet the criteria of the total load specifically as well as to increase the longitudinal stability margin.

3.2.1 Force and moment analysis

In this section, the conceptual aerodynamic shape is analyzed for the feasibility of the proposed design. Forces and moments acting in the longitudinal plane of the configuration are drawn in Fig. 4.

Here, c is the mean zero lift chord of the bottom wing, and h and $h_{ac,w1}$ are the distance of the centre of gravity of the whole system and aerodynamic centre of the bottom wing, respectively, from the leading edge of the bottom wing in a fraction of chord length of the bottom wing. z_{w1} denotes the vertical distance of the centre of gravity from the mean zero lift chord of the bottom wing in a fraction of bottom chord length. $M_{ac,w1}$ and $M_{ac,w2}$ are the moment of the top and bottom wing of their aerodynamic centre, respectively. L_{w1} , L_{w2} , D_{w1} , and D_{w2} are the lift and drag forces acting on top and bottom wing. ϵ is the downwash angle, and α_{w1} and $\alpha_{w1} - \epsilon$

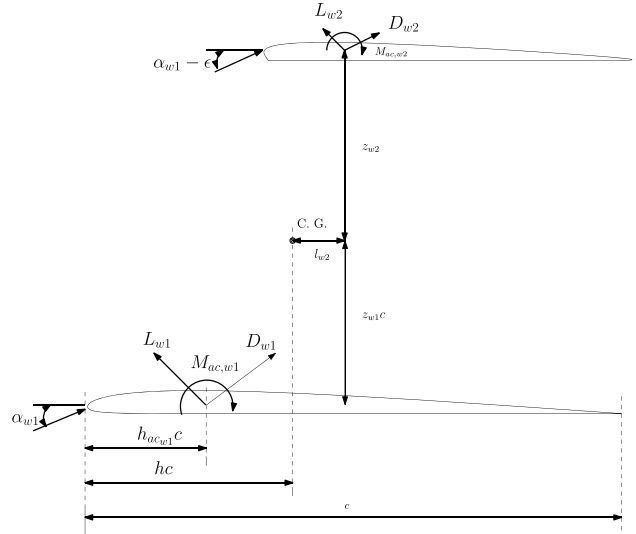


Fig. 4 Forces and moments in the longitudinal plane

are the absolute angle of attack of the bottom wing and top wing, respectively.

Therefore, the total moment about the MAV CG due to the forces acting on the bottom wing is given by

$$M_{cg,w1} = M_{ac,w1} + L_{w1} \cos \alpha_{w1} (hc - h_{ac,w1}c) + D_{w1} \sin \alpha_{w1} (hc - h_{ac,w1}c) + L_{w1} \sin \alpha_{w1} z_{w1}c - D_{w1} \cos \alpha_{w1} z_{w1}c \quad (1)$$

For the analysis purposes, let us assume α_{w1} to be small. Therefore, $\cos \alpha_{w1} \approx 1$; $\sin \alpha_{w1} \approx \alpha_{w1}$. Then, the total moment can be simplified as follows:

$$M_{cg,w1} = M_{ac,w1} + L_{w1}(hc - h_{ac,w1}c) + D_{w1}\alpha_{w1}(hc - h_{ac,w1}c) + L_{w1}\alpha_{w1}z_{w1}c - D_{w1}z_{w1}c \quad (2)$$

The pitching moment, and lift and drag coefficient for bottom wing are defined as follows:

$$C_{M,cg,w1} = \frac{M_{cg,w1}}{q_\infty S_{w1}c}; C_{M,ac,w1} = \frac{M_{ac,w1}}{q_\infty S_{w1}c}; C_{L,w1} = \frac{L_{w1}}{q_\infty S_{w1}}; C_{D,w1} = \frac{D_{w1}}{q_\infty S_{w1}},$$

where q_∞ is the dynamic pressure and S_{w1} is the surface area of the bottom wing. Dividing Eq. (2) by $q_\infty S_{w1}c$, we get

$$C_{M,cg,w1} = C_{M,ac,w1} + (C_{L,w1}\alpha_{w1} - C_{D,w1})z_{w1} + (C_{L,w1} + C_{D,w1}\alpha_{w1})(h - h_{ac,w1}). \quad (3)$$

Similarly, the total moment about CG due to forces acting on the top wing is given by

$$M_{cg,w2} = M_{ac,w2} - l_{w2}(L_{w2} \cos(\alpha_{w1} - \epsilon) + D_{w2} \sin(\alpha_{w1} - \epsilon)) - z_{w2}L_{w2} \sin(\alpha_{w1} - \epsilon) + z_{w2}D_{w2} \cos(\alpha_{w1} - \epsilon), \tag{4}$$

where z_{w2} and l_{w2} are the vertical and horizontal distance of the aerodynamic centre of the top wing from the CG of the MAV.

The various aerodynamic coefficient for top wings are defined as

$$C_{L,w2} = \frac{L_{w2}}{q_{\infty}S_{w2}}; C_{D,w2} = \frac{D_{w2}}{q_{\infty}S_{w2}}; C_{M,cg,w2} = \frac{M_{cg,w2}}{q_{\infty}S_{w1}c}; C_{M,ac,w2} = \frac{M_{ac,w2}}{q_{\infty}S_{w1}c},$$

where S_{w2} is the surface area of the top wing. With the assumption that the magnitude of $\alpha_{w1} - \epsilon$ is small, the total moment due to forces acting on top wing about the CG can be approximated as

$$M_{cg,w2} = M_{ac,w2} - l_{w2}(L_{w2} + D_{w2}(\alpha_{w1} - \epsilon)) - z_{w2}L_{w2}(\alpha_{w1} - \epsilon) + z_{w2}D_{w2}. \tag{5}$$

After dividing the Eq. (5) with $q_{\infty}S_{w1}c$, we get

$$C_{M,cg,w2} = C_{M,ac,w2} - \frac{l_{w2}L_{w2}}{q_{\infty}S_{w1}c} - \frac{l_{w2}D_{w2}(\alpha_{w1} - \epsilon)}{q_{\infty}S_{w1}c} - \frac{z_{w2}L_{w2}(\alpha_{w1} - \epsilon)}{q_{\infty}S_{w1}c} + \frac{z_{w2}D_{w2}}{q_{\infty}S_{w1}c}. \tag{6}$$

Using the aerodynamic coefficient, the above equation can be simplified as follows:

$$C_{M,cg,w2} = C_{M,ac,w2} - \frac{l_{w2}S_{w2}}{S_{w1}c} C_{L,w2} - \frac{l_{w2}S_{w2}}{S_{w1}c} C_{D,w2}(\alpha_{w1} - \epsilon) - \frac{z_{w2}S_{w2}}{S_{w1}c} C_{L,w2}(\alpha_{w1} - \epsilon) + \frac{z_{w2}S_{w2}}{S_{w1}c} C_{D,w2}. \tag{7}$$

In this case, we will define the wing volume ratio W_H similar to tail volume ratio of normal aircraft as, $W_H = \frac{l_{w2}S_{w2}}{S_{w1}c}$. Also, $f = \frac{z_{w2}}{l_{w2}}$. Therefore

$$C_{M,cg,w2} = -W_H C_{L,w2} - W_H C_{D,w2}(\alpha_{w1} - \epsilon) - W_H f C_{L,w2}(\alpha_{w1} - \epsilon) + W_H f C_{D,w2} + C_{M,ac,w2}. \tag{8}$$

For the entire system, we will define the pitching moment coefficient as follows: $C_{M,cg} = \frac{M_{cg}}{q_{\infty}S_{w1}c}$, where M_{cg} is the total moment about the centre of gravity. Therefore

$$C_{M,cg} = C_{M,cg,w1} + C_{M,cg,w2}. \tag{9}$$

For the system to be stable in longitudinal plane, it should satisfy the following two criteria [36]:

- $C_{M,0}$ must be positive.
- $\frac{\partial C_{M,cg}}{\partial \alpha_a}$ must be negative.

Here, α_a is the absolute angle of attack of whole body, $C_{M,0}$ is the moment coefficient about the centre of gravity at zero lift, and $\frac{\partial C_{M,cg}}{\partial \alpha_a}$ is the slope of the $C_{M,cg}$ vs α_a curve. In this case, we will assume, $\alpha_a \approx \alpha_{w1}$. Let a_{w1}, a_{w2} be the slope of the lift curve of bottom wing and top wing. Then, $C_{L,w1} = a_{w1}\alpha_{w1}$; $C_{L,w2} = a_{w2}(\alpha_{w1} - \epsilon)$. Hence

$$C_{M,0} = C_{M,ac,w1} - z_{w1}([C_{D,w1}]_{\alpha_{w1}=0}) + C_{M,ac,w2} + \epsilon W_H a_{w2} + \epsilon W_H ([C_{D,w2}]_{\alpha_{w1}=0}) + W_H f ([C_{D,w2}]_{\alpha_{w1}=0}) - \epsilon^2 W_H f a_{w2}, \tag{10}$$

where $[C_{D,w1}]_{\alpha_{w1}=0}$ means the value of $C_{D,w1}$ when value of α_{w1} is zero. $\frac{\partial C_{M,cg}}{\partial \alpha_{w1}}$ can be expressed as

$$\frac{\partial C_{M,cg}}{\partial \alpha_{w1}} = \frac{\partial C_{M,cg,w1}}{\partial \alpha_{w1}} + \frac{\partial C_{M,cg,w2}}{\partial \alpha_{w1}}. \tag{11}$$

Neglecting the lower magnitude drag terms

$$\frac{\partial C_{M,cg,w1}}{\partial \alpha_{w1}} = a_{w1}(h - h_{ac,w1}) + 2a_{w1}\alpha_{w1}z_{w1}. \tag{12}$$

Similarly

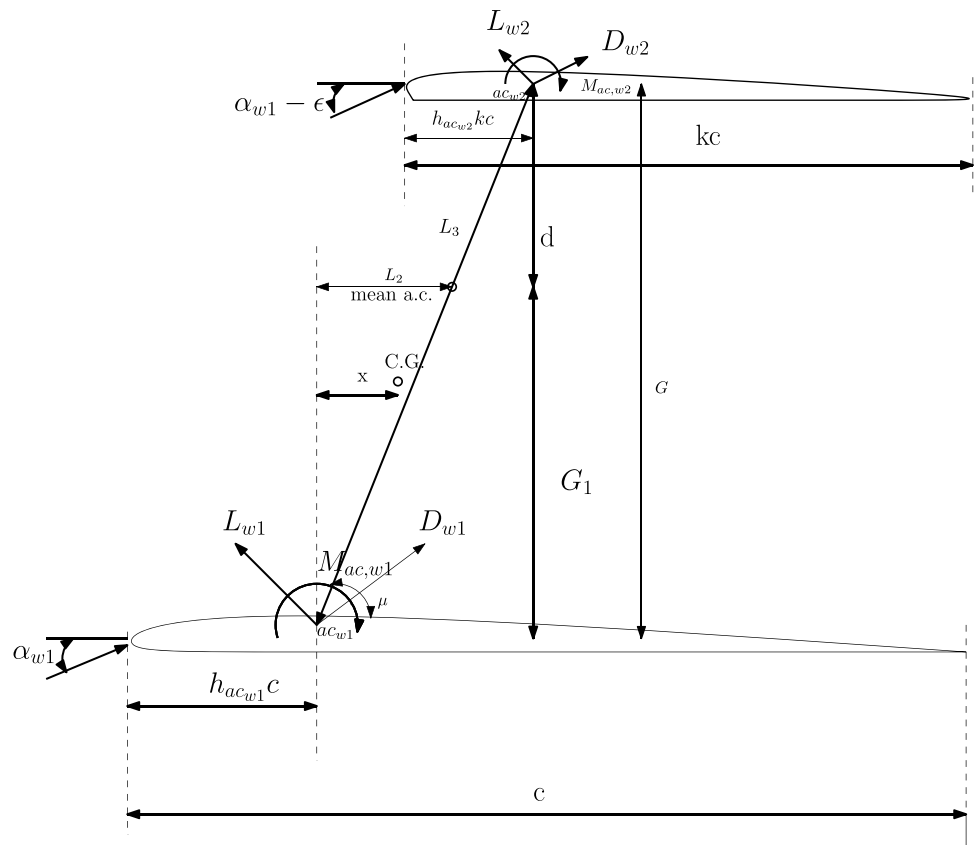
$$\frac{\partial C_{M,cg,w2}}{\partial \alpha_{w1}} = -W_H a_{w2} - 2W_H f(\alpha_{w1} - \epsilon)a_{w2}. \tag{13}$$

Therefore

$$\frac{\partial C_{M,cg}}{\partial \alpha_{w1}} = a_{w1}(h - h_{ac,w1}) + 2a_{w1}\alpha_{w1}z_{w1} - W_H a_{w2}(1 + 2f(\alpha_{w1} - \epsilon)). \tag{14}$$

As evident from Eq. (10), $C_{M,0}$ can be made positive by choosing $C_{M,ac,w1}$ and $C_{M,ac,w2}$ closer to zero, making z_{w1} as small as possible and W_H as high as possible. Equivalently, the airfoils should be of very low pitching moment, the centre of gravity should be closer to the bottom wing, and the top wing should be selected for higher W_H . From Eq. (14), it is clear that $\frac{\partial C_{M,cg}}{\partial \alpha_a}$ can be made negative with higher value of W_H and smaller value of z_{w1} . Equivalently, the top wing needs to be optimum for a higher W_H value, and the overall system centre of gravity needs to be kept closer to the

Fig. 5 Longitudinal stability analysis of whole system



bottom wing. From the above analysis, the following conclusions can be made:

- Airfoil pitching moment should be small.
- CG should be kept near to bottom chord line.
- The top wing should be designed for a higher value of W_H .

3.2.2 Analysis of chord length of top wing

In this section, a tentative range of chord length of the top wing is determined from the point of view of longitudinal static stability. For longitudinal stability, the centre of gravity should be in front of the neutral point. The location of the neutral point would be around the mean aerodynamic centre of the complete system. Hence, in this case as per the Fig. 5, L_2 should be greater than x .

Here, L_2 and x are the horizontal distance of the mean aerodynamic centre and the centre of gravity from the bottom wing's aerodynamic centre. In Fig. 5, k is the ratio of the chord length of top wing to bottom wing, and G_1 is the vertical distance between the mean aerodynamic centre of the whole system from the zero lift chord line of the bottom wing. We have

$$L_2 = G_1 \cot \mu,$$

where G is the vertical distance between zero lift chord line of the top wing and bottom wing and μ , is the angle between the bottom chord and line joining the aerodynamic centre of the top wing and bottom wing. The approximate mean aerodynamic centre of the whole biplane from the zero lift chord line of the bottom wing can be calculated as

$$G_1 = \frac{GL_{w2}}{L_{w2} + L_{w1}},$$

we have, $L_{w2} = C_{L,w2} q_\infty S_{w2}$ and $L_{w1} = C_{L,w1} q_\infty S_{w1}$. we will assume that $C_{L,w2} \approx C_{L,w1}$. Considering the span is same for top and bottom wing

$$G_1 = \frac{GC_{L,w2} q_\infty bkc}{C_{L,w2} q_\infty bkc + C_{L,w1} q_\infty bc}.$$

After simplification, we get

$$G_1 = \frac{kc}{kc + c} G.$$

Therefore

$$L_2 = \frac{k}{k+1} G \cot \mu.$$

Also,

$$\cot \mu = \frac{\sqrt{L_3^2 - G^2}}{G},$$

where L_3 is the distance between the aerodynamic centre of the top wing and bottom wing. As a result

$$L_2 = \frac{Gk}{k+1} \frac{\sqrt{L_3^2 - G^2}}{G},$$

L_3 can be expressed as

$$L_3^2 = G^2 + \left((c - h_{ac_{w1}} c) - (kc - h_{ac_{w2}} kc) \right)^2.$$

Considering the fact that the values of $h_{ac_{w1}}$ and $h_{ac_{w2}}$ are approximately 0.25, the value of L_3 can be approximated as

$$L_3^2 = G^2 + \left(\left(c - \frac{c}{4} \right) - \left(kc - \frac{kc}{4} \right) \right)^2,$$

so

$$\sqrt{L_3^2 - G^2} = \frac{3}{4}(c - kc).$$

Therefore,

$$L_2 = \frac{k}{1+k} \frac{3}{4}(c - kc).$$

Hence, for longitudinal stability

$$\left(\frac{k}{1+k} \right) \frac{3}{4}(c - kc) > x. \tag{15}$$

Equivalently, $\frac{k(1-k)}{1+k} > \frac{4x}{3c}$. If we restrict maximum value of $x = 0.1c$, the above equation reduces to $\frac{k(1-k)}{1+k} > 0.133$. Therefore, $k - k^2 > 0.133(1+k)$, which results in $0.19 < k < 0.66$. As the increment of load-carrying capacity is considered as main design objectives, the value of k needs to be chosen on the higher side.

In traditional tail design, the horizontal tail's primary function is to balance the moment in the longitudinal plane. In this case, the top wing will generate a significant amount of extra lift, and it will also help in balancing the moment. As evident from the analysis, this special configuration will allow a larger range of CG location variations, which is crucial to incorporate the extra components of the vision systems. Additionally, this will improve stability. The whole configuration can also be thought of as an equivalent canard configuration, where the top wing is the main wing, and the bottom wing is similar in functionality as the canard.

Passive techniques such as vertical tail design incorporating the effects of counter-torque and asymmetric weight distribution about the x-axis are considered for balancing the counter-torque, since active balancing of counter-torque using the control surfaces may be prohibitive.

4 Preliminary design

4.1 Bottom wing design

In the case of MAV, wing design is the most important aspect of the design process, and its design requirement includes performance requirement, stability criteria, structural considerations, ease of manufacturing, and placing of payload and electronic components. Wing shape, airfoil, and aspect ratio need to be selected considering the complex aerodynamics of low Reynolds number [37–40].

In this case, the aspect ratio of 1.0–1.25 is the region of interest. While the elliptical planform has better aerodynamic performance due to its elliptical lift distribution, the construction is especially difficult for the MAV class of vehicles. Wind tunnel results at Reynolds number of 10^5 show that, around aspect ratio of 1.0–1.25, lift coefficient for rectangular planform is higher than other planforms like Zimmerman, elliptical, and inverse Zimmerman while the drag coefficient is comparable; however, the maximum lift coefficient and the angle of attack at which maximum lift coefficient occurs is comparatively lower for rectangular planform [41]. Also, in the case of rectangular planform, components can be placed comfortably toward the leading edge to obtain a favourable stability margin. Since our design requirement is to increase the total lift as much as possible, a rectangular planform seems to be the best choice.

4.1.1 Airfoil selection

As seen from the force and moment analysis of the basic configuration, the airfoil needs to be selected with almost zero pitching moment, with the lift coefficient as high as possible. Different airfoils with low pitching moment are considered for preliminary analysis, and based on their aerodynamic properties, rank is determined. Initially, airfoils are ranked separately at velocities 8 m/s, 10 m/s, and 12 m/s based on their values of C_L and C_m at angle of attack (α) for which $\left(\frac{C_L}{C_D}\right)$ is maximum. Then, a score is developed based on their rank in both categories. Equal weight is given to both categories. Let say the rank of an airfoil S5010 at 8 m/s is f_1 and f_2 in both categories. Then, the score of airfoil S5010 at 8 m/s is obtained as follows:

$$f_{s5010} = -(0.5f_1 + 0.5f_2).$$

Table 4 3D analysis of airfoil for rectangular platform

Component	$C_{L_{max}}$	α	$\frac{C_L}{C_D}$	C_m	Rank
S5010	0.64	37	3.65	-0.122	3
E325	0.63	38	3.67	-0.092	3
MH60	0.641	37	3.715	-0.123	1
ESA40	0.628	38	3.65	-0.084	4
EH1590	0.641	37	3.71	-0.123	2

Airfoils are ranked based on their individual score. An airfoil could have a higher rank in the category of 8 m/s, 10 m/s and lower rank in the category of 12 m/s compared to another airfoil. Therefore, a global score is formulated to resolve the conflicts. The global score of each airfoil is provided based on their rank for 8 m/s, 10 m/s, and 12 m/s

$$\text{Global score of each airfoil} = -(0.3R_8 + 0.4R_{10} + 0.3R_{12}),$$

where R_8 , R_{10} , and R_{12} are the rank of airfoil at 8 m/s, 10 m/s, and 12 m/s, respectively. More weight is given to 10 m/s as the nominal velocity of the MAV is expected to be 10 m/s. The soft stalling characteristic of the airfoil and bottom shape of the airfoil for comfortable component placement are also considered for airfoil selection. S5010, E325, MH60, ESA40, and EH1590 airfoils are further selected for 3D analysis. In 3D analysis, the aerodynamic analysis is performed with a rectangular planform for different airfoils. Initially, each airfoil is ranked based on the C_L , $\frac{C_L}{C_D}$, C_m at an angle of attack for which the value of C_L is maximum. Then, a score is provided based on their rank as follows:

$$\text{Airfoil score} = -(0.5R_1 + 0.25R_2 + 0.25R_3),$$

where R_1 is the rank while comparing C_L , R_2 is the rank while comparing $\frac{C_L}{C_D}$ and R_3 is the rank while comparing C_m . The results of the 3D analysis are shown in Table 4. After 3D analysis of these airfoils for rectangular planform wings, MH-60 is found to be better. Although the aerodynamic performance of MH-60 is better, its maximum thickness of 10.1% is not enough to accommodate the components. Therefore, a modified version of MH-60 is designed with a

maximum thickness of 12% under the assumption that the aerodynamic performance will not vary significantly from the original design. The thickness ratio of 12% is considered by taking into account the ease in placement of components and burden of structural load. This modified MH-60 airfoil is selected for the bottom wing.

4.1.2 Aspect ratio

For rectangular planform, aerodynamic characteristics of the wing are analyzed in Table 5. The analysis is done on rectangular planform of airfoil MH-60 having a thickness ratio of 12% for nominal velocity for 10 m/s. The analysis is done for the angle of attack of 0° – 50° . The span length is kept at 15 cm, and different chord length is considered for analysis of aspect ratio. The aspect ratio of 1.25 will have better aerodynamic performance. However, the total load-carrying capacity is less. Also, a higher wing chord will allow more CG variation for the longitudinal stability requirement and hence better static margin. The aspect ratio of 1.07 is selected considering these two factors along with the maximum dimension restriction.

4.2 Top wing design

The top wing and bottom wing need to be designed separately, considering the particular aspects involved in each wing. In the case of the design of the top wing, the main criteria are to increase the wing volume ratio (W_H), lifting capacity while having a small pitching moment and self-weight.

As per force and moment analysis in Sect. 3.2.1, the airfoil must be of low pitching moment. Along similar lines discussed in the bottom wing design, the shape of the top wing is selected as a rectangular planform with the MH-60 airfoil. Considering the structural design point of view, and also from the analysis in Sect. 3.2.1, most of the components are need to be placed in the bottom wing to keep the CG near to bottom chord line. Therefore, the maximum thickness of 9% seems to be adequate considering the trade-off between ease of manufacturing and its self-weight. Therefore, a

Table 5 Aspect ratio (AR) analysis for rectangular platform

AR	Span	Chord	Area	$C_{L_{max}}$	$(\frac{C_L}{C_D})_{max}$	Lift	ac distance from leading edge (mm)
(-)	(mm)	(mm)	(cm ²)	(-)	(-)	(N)	
1.0	150	150	225	0.602	6.81	0.678	37.5
1.07	150	140	210	0.641	6.87	0.673	35
1.15	150	130	195	0.685	6.96	0.669	32.5
1.25	150	120	180	0.74	7.04	0.664	30
1.36	150	110	165	0.795	7.10	0.658	27.5

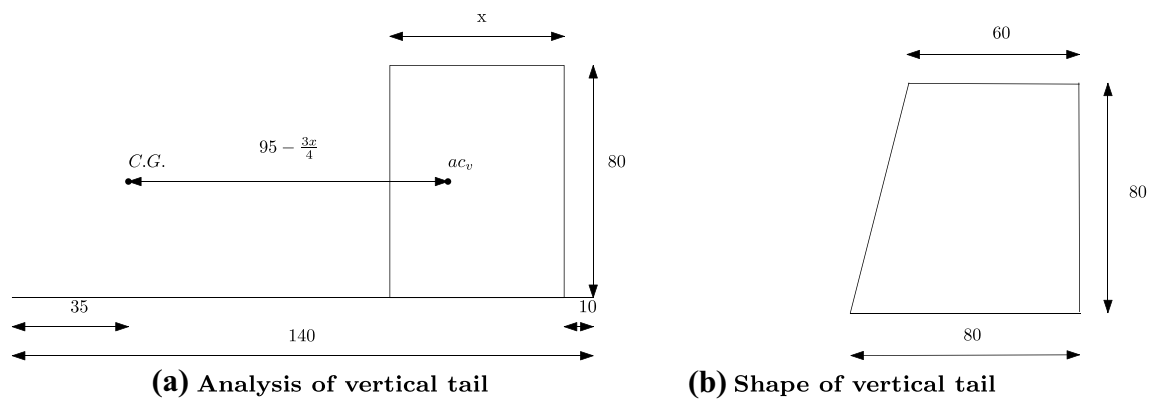


Fig. 6 Vertical tail

modified version of MH-60 having a maximum thickness of 9% is considered.

The span length is selected as 150 mm as the bottom wing to get the maximum utilization of the available area to increase the payload of MAV. As per analysis in Sect. 3.2.2, the chord length of the top wing must be 0.19–0.66 in the fraction of the chord length of the bottom wing for a stability point of view. The increment of the load-carrying capacity of MAV is the crucial criterion for the overall MAV design. Therefore, the value of k is chosen on the higher side as 0.6. Therefore, the chord length is selected as 85 mm, which results in an aspect ratio of 1.76.

4.3 Vertical tail and winglet design

Apart from directional trim and stability, the vertical tail needs to balance some part of the rolling moment generated due to the counter-torque of the motor. The counter-torque is large in MAV due to its low moment of inertia compared to bigger UAVs, and some part of it needs to be balanced by aerodynamic design. Otherwise, it is difficult to balance this through control surfaces actively. The asymmetric airflow over the wing due to propeller rotation can be used to generate the rolling moment opposite to the counter-torque by exposing the vertical tail to propeller wash. The vertical tail can be placed in the centre of the wing to get the advantages of these effects. The design of having a twin vertical tail on the side edge was not effective. During flight testing, it was noticed that the counter-torque was too large to be balanced with the available control surfaces in the latter case. Therefore, the vertical tail is placed in the centre of the wing.

The top wing is placed on top of the vertical tail resembling a T configuration. This configuration is favourable for reducing the interference between the top and bottom planes and the manufacturing perspective.

The MAV is considered as a home build category for the selection of vertical tail volume ratio. In this case, the

vertical tail volume ratio of 0.05 is selected rather than the recommended 0.04 as the larger area of the vertical tail will help in balancing the counter-torque. The height of the vertical tail is selected as 80 mm by considering the interference between the top and bottom wing, structural load. The area of wing (S_W) is considered as the total area of the top and bottom wing, and the wing chord (c_W) is considered as the chord of the bottom wing.

From Fig. 6a, the tail volume ratio is given by

$$\frac{S_{V_t} l_{V_t}}{S_W c_W} = \frac{80x \times (95 - \frac{3x}{4})}{33750 \times 140} = 0.05, \quad (16)$$

where S_{V_t} is tail area and l_{V_t} is tail moment arm. The maximum possible value of x is obtained as 71.9 mm by solving Eq. (16). Also, considering the structural point of view, the shape of the tail is considered as a trapezoid having sides 80 mm and 60 mm with a height of 80 mm. The longer vertical tail base is required to provide strong structural support to the vertical tail itself as well as the top wing; the geometry of the vertical tail is shown in Fig. 6a, b. A symmetric airfoil, NACA 0010 is chosen for vertical tail considering manufacturing perspective and to avoid the moments due to non-symmetric airfoil.

The winglet is a surface that can increase both the overall lift coefficient and the vehicle's rolling stability while reducing the induced drag; this advantage comes at the expense of an increase in the parasitic drag and the structural load. The quantification of this trade-off is complex for this class of vehicles. For this MAV, winglets can be made from thin sheets of laminate fibre materials, having no effect on the structural load. Since the main design criteria are to increase the payload capacity, winglets are provided. The position of the winglets is chosen at the rearward end of the wing, which offers better aerodynamic performance. A mathematical analysis considering the trade-off of lift coefficient, vehicle rolling stability, parasite drag, and structural load

Table 6 Aileron design specification

Control surface	Class	Acceptability	Phase	Time to achieve 30° bank angle
Aileron	IV	1	C	1.3 s

will provide a better estimate of the size of the winglets. However, in this case, the shape of the winglets is chosen based on the manufacturing perspective and shape of available laminate fibre sheets. The winglet is chosen in the shape of a right angle triangle which has a base of 45 mm and a height of 30 mm, and it is provided on both the top and the bottom wing.

4.4 Control surface design

It is preferable to have a number of control surfaces as disturbance attenuation and tracking the performance of MAV can be enhanced with more inputs. However, configurations, such as elevator-aileron, elevator-rudder, elevon, etc., are sufficient for control of the MAV. As space and weight budget are constrained, elevon configuration is selected over other configurations.

The effectiveness of the control surface will be high if it is placed within propeller wash; hence, small area of control surfaces will be enough. However, this will also increase the sensitivity of the control surfaces. If the control surface is placed in the propeller wake, i.e., on the main wing, with the small change in the control surface, the flow pattern on the main wing will change substantially. Hence, the control surface is placed on the top wing considering all these effects.

The control surfaces ought to be designed considering the handling quality as per aircraft weight, manoeuvrability, flight phase, ease of flight, and flight safety. Since there is no direct standard available for the MAV class of vehicle, the most similar category from the available standard is selected for the control surface design. The MAV is considered Class-IV, whose characteristics are “Small, light aircraft” for assessing handling quality as per MIL-F8785C. In terms of ease of flight and flight safety, the level of acceptability is considered as one.

4.4.1 Aileron design

Aileron is designed as per the design approach discussed in [21]. The landing phase is considered as the critical phase of the MAV mission for the aileron design; hence, the design is carried out for phase C as per MIL-F8785C. In this case, the design requirement in terms of time to achieve the specified bank angle is specified in Table 6.

Table 7 Control surface requirement

Parameter	Lifting surface	Elevator	Aileron
Area (mm ²)	337.5	50.62–135	10.12–40.5
Span (mm)	150	120–150	30–60
Chord (mm)	140	28–56	21–42

The control surface size requirement as per specification is mentioned in Table 7. Along with these requirements, the factors such as the minimum gap between the control surfaces and the maximum size restrictions on MAV need to be considered for design. Maximum allowable deflection for an aileron is considered as 20°. The time required to achieve the 30° bank angle is calculated using the rate of roll rate produced by the rolling moment to reach the steady-state roll rate; where MAV achieves the steady-state roll rate when the moment generated due to aileron becomes equal to the moment due to drag due to rolling motion. After a few design iterations, the size of each aileron is selected as the span of 70 mm and chord of 26 mm.

4.4.2 Elevator design

The elevator deflection (δ_e) required for longitudinal trim is given by [21]

$$\delta_e = - \frac{\left(\frac{TZ_T}{q_\infty S c} + C_{m_0} \right) C_{L_\alpha} + (C_L - C_{L_0}) C_{m_\alpha}}{C_{L_\alpha} C_{m_{\delta_e}} - C_{m_\alpha} C_{L_{\delta_e}}}, \tag{17}$$

where T is engine thrust; Z_T is the moment arm between motor axis and centre of gravity; C_{m_0} is the pitching moment coefficient when angle of attack (α) = pitch rate (q) = $\delta_e = 0$; C_{m_α} is the slope of pitching moment coefficient vs angle of attack; C_{L_α} is the slope of lift coefficient vs angle of attack; C_L is the total lift coefficient; C_{L_0} is the value of lift coefficient when $\alpha = q = \delta_e = 0$; $C_{L_{\delta_e}}$ is the slope of lift coefficient vs elevator deflection. In this case, Z_T is zero as motor axis is passed through the centre of gravity. Considering the approximate value of the aerodynamic coefficients from the preliminary XFLR analysis (discussed in Sect. 4.5), the elevator angle of trim is obtained as follows. For

$$C_{m_0} = 0.062, C_{L_\alpha} = 2.29, C_L = 0.55, C_{L_0} = -0.015$$

$$C_{m_\alpha} = -0.14, C_{m_{\delta_e}} = -0.81, C_{L_{\delta_e}} = 0.65$$

$$\delta_e = 1.45^\circ < 20^\circ.$$

Therefore, the required elevator angle for trim is less than the maximum allowable elevator deflection. The details of the model shape are shown in Table 8.

Table 8 Model specifications

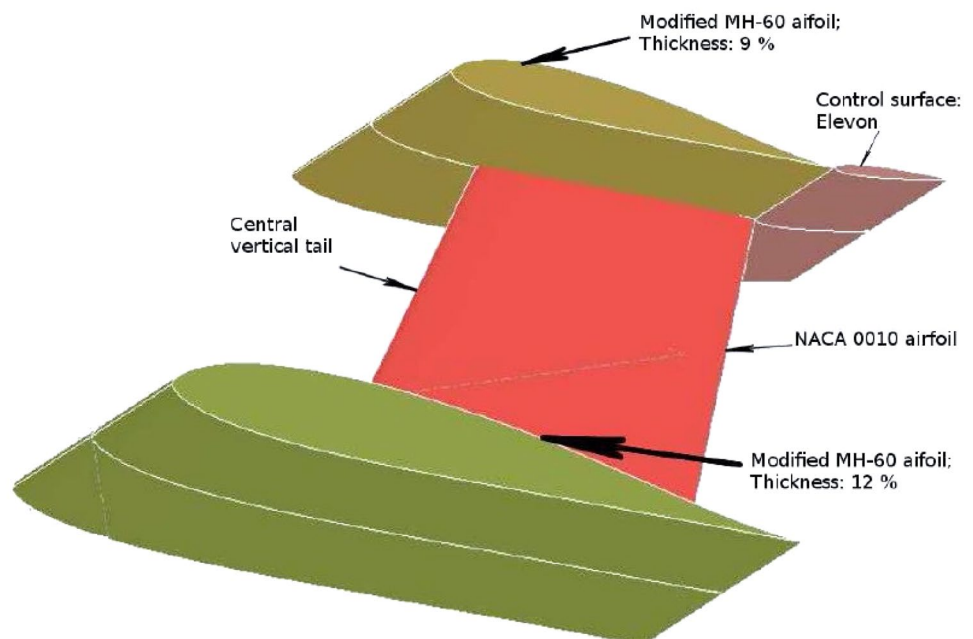
Parameter	Specifications
Top wing span	150 mm
Bottom wing span	150 mm
Top wing chord	85 mm
Bottom wing chord	140 mm
Top wing airfoil	Modified MH-60
Bottom wing airfoil	Modified MH-60
Vertical tail height	80 mm
Vertical tail area	5600 mm ²
Planform	Rectangular
Elevon	75 × 26 mm

4.5 Aerodynamic analysis using XFLR software

The aerodynamic performance and stability of the conceptual model are carried in XFLR software before proceeding toward the detailed design of the system. The MAV configuration after the preliminary design is shown in Fig. 7.

The analysis is carried out using the Vortex lattice method (VLM) for a fixed lift of 100 g. Since the propeller flow contributes toward some percentage of total lift, the designed lift for the XFLR analysis is considered 100 g instead of 110 g, assuming that 10% additional lift from propeller flow. The horizontal position of CG is kept at a distance of 35 mm from the leading edge of the bottom wing airfoil and 25 mm from the mean chord line of the bottom wing.

Fig. 7 Proposed MAV configuration



Variation of lift force coefficient and drag force coefficient are plotted in Fig. 8a, b. As per static stability requirement, the value of C_{m_α} and C_{l_β} should be negative; $C_{M,0}$ and C_{n_β} should be positive. Clearly, from Fig. 8c–e, the system satisfies the stability requirement as the sign of the stability derivatives matches with the criteria. In this case, the value of stability derivatives are as follows:

$$C_{m_\alpha} = -0.14; C_{l_\beta} = -0.081; C_{n_\beta} = 0.095.$$

As per Fig. 8c, the trim angle of attack for this MAV is around 21°. The required MAV velocity with the variation of the angle of attack is shown in Fig. 8f. Therefore, the velocity corresponding to the trim angle of attack is about 11 m/s, which is achievable for this MAV. Hence, this MAV configuration is feasible. In XFLR analysis, the effect of motor-propeller is not included; however, the effect of motor counter-torque and propeller flow will have a significant contribution to the overall MAV dynamics [42–44]. Immersion of the wing-body on propeller slipstream is favourable for an extra lift while causing detrimental effects on drag and pitching moment [45, 46]. Since the basic system is stable, it is possible that the overall system can be made stable if the destabilizing effects of counter-torque and propeller flow are kept under a reasonable limit. At this stage, CFD analysis of the proposed configuration is performed and found that the proposed configuration can provide the lift required for desired take-off mass of 110 g.

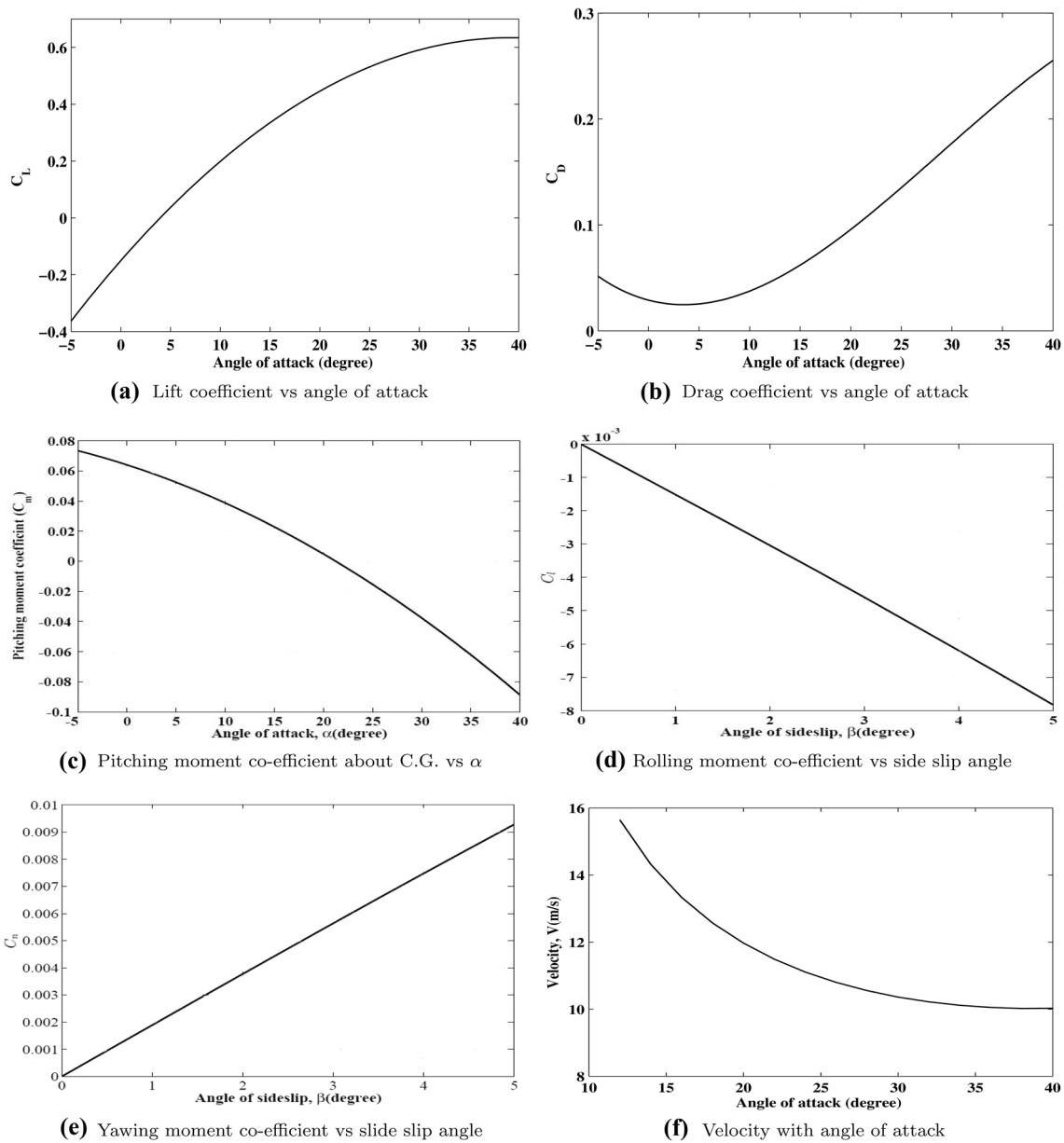


Fig. 8 Force and moment coefficient

5 Detailed design

5.1 Propeller and motor

The front location of the motor is chosen as it will move the overall system CG toward the leading edge, and the propeller wash will increase the lifting capability along with balancing the counter-torque; these advantages of propeller wash outweigh the disadvantages like destabilizing lateral and longitudinal moments. Current drawn and counter-torque of different motor-propeller combinations capable of providing enough thrust are experimentally tested. Finally, the AP-05

motor with the GWS 5 × 3 propeller is selected. With this motor-propeller combination, dynamic thrust (T_A) of MAV

Table 9 Propeller motor dynamic thrust

Motor RPM	Dynamic thrust (g)
10,500	25.30
11,000	31.55
11,500	38.26
12,000	45.43
12,500	53.06
13,500	69.70

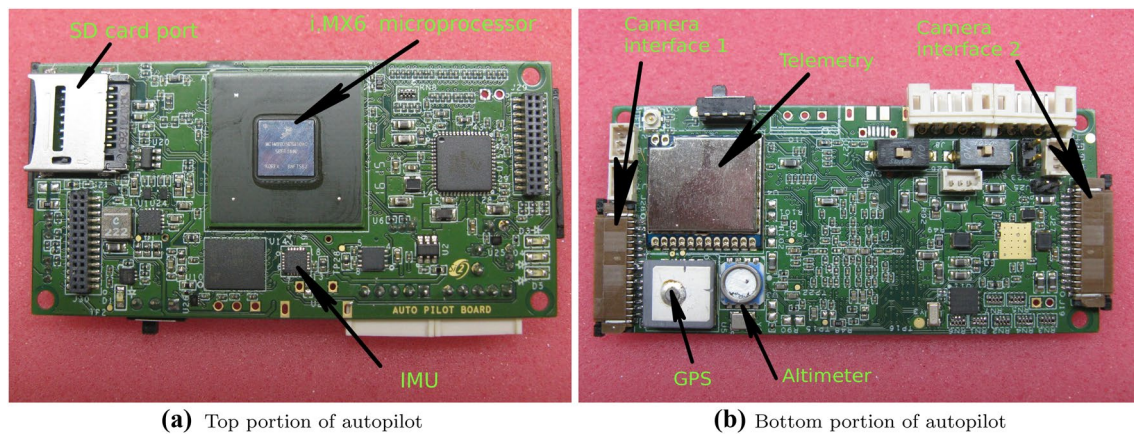


Fig. 9 Autopilot top and bottom view

Table 10 Autopilot details

Component	Description	Component	Description
Weight	16 g	Size	35 × 65 mm
Main controller unit	i.MX6 Freescale processor	RAM	512 MB
IMU	MPU-9250 (9 axis)	Altimeter	MS 5803-01BA
GPS	ORG-1411	Camera interface	CSI
Flash	8 Mbit	Micro SD card	8 GB

is tabulated in Table 9 [47]. From Fig. 8b, the drag force corresponding to 11 m/s trim velocity and an angle of attack of 21° is 26.54 g. Therefore, from Table 9, the motor RPM will be around 10,500–11,000.

5.2 Autopilot hardware

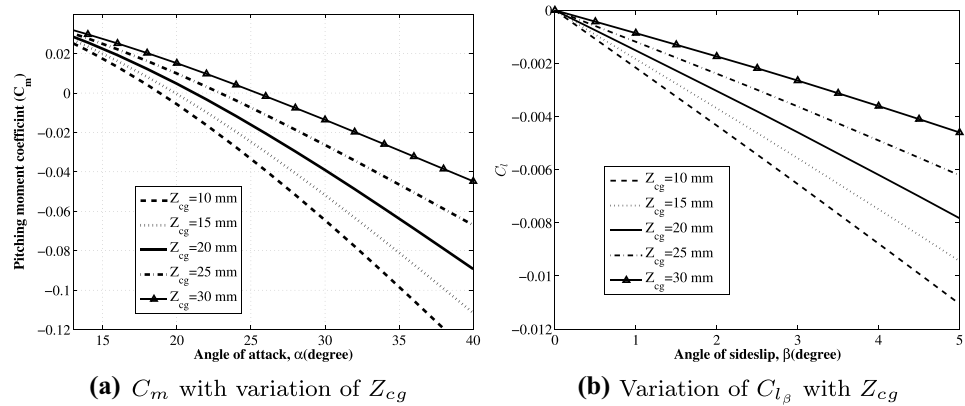
In the case of MAV, it is very difficult to incorporate two separate modules for low-level tasks and high-level tasks due to weight, space, and power constraints. Therefore, the autopilot is developed as a single lightweight module that is capable of performing high-level tasks like image processing as well as low-level tasks like the generation of the control command. The expected computational load on the system will be higher due to the processing of large data involved in image processing tasks. The feasibility study of the main control unit with a microcontroller, microprocessor, and FPGA is carried out. The size and weight of the autopilot will be less in the case of the microcontroller; however, its computational power is low. The FPGA-based system can perform fast image processing, but the weight and power requirement of the system will be too high to incorporate into the weight budget. Therefore, the microprocessor-based main control unit is selected considering the trade-off between weight and computational power. The

pictures of the autopilot are shown in Fig. 9a, b. The details of the autopilot are presented in Table 10. The other major electronic components are YEP-7A electronic speed controller, HobbyKingTM HK15318B servos, 433 MHz telemetry module, and Raspicam camera module.

5.3 Structural design

Load distributions and crashworthiness during landing are the two most important points for structural design. The design has to guarantee that any impact load during landing should be distributed throughout the whole structure to ensure minimum damage to the vehicle. The top plane must be made lighter to reduce the weight burden on the vertical tail; else, the requirement of the strong vertical tail will cause the overall CG to move rearward, which, in turn, will reduce the static margin. The variation of $C_{M, cg}$, C_{l_β} is plotted with the vertical distance of CG from the bottom chord line (Z_{cg}) in Fig. 10a, b. It is clear from the Fig. 10a that low value of Z_{cg} is preferable as it will require less trim velocity. Generally, coupled models of these types of vehicles are spirally unstable, so it is preferable to use more negative C_{l_β} for better spiral stability. However, higher C_{l_β} will deteriorate the dutch roll stability. In this case, the stability of the spiral

Fig. 10 Variation of stability derivatives with Z_{cg}



modes is given more importance. Clearly, spiral stability improves with low value of Z_{cg} as in Fig. 10b. Therefore, the components are loaded mostly in the bottom wing to make Z_{cg} as low as possible.

The top wing is made of a very light material (EPP—density of 20 kg/m^3), and only lightweight servos are placed in the top wing. The vertical tail is made of depron with aero ply strip reinforcement. A load of the top plane is transferred to the bottom plane through this vertical aero ply strip. The bottom wing is made of a box-like structure with four airfoils placed in the longitudinal direction. These four airfoils are connected to a carbon rod to make an integrated structure. The vertical tail with a top plane is connected strongly to middle airfoils through horizontal ribs. In this way, it is ensured that any external load during landing is properly distributed throughout the body.

The ribs of the bottom airfoil are cut in a laser cutting machine from a 1 mm-thick aeroply. The top airfoils are made from lightweight EPP using hot-wire cutter. Initially, a frame structure is made with four airfoils using a carbon tube; and the outer surface is covered with 1 mm-thick balsa strip. The vertical tail is connected with the frame structure of the bottom wing with side ribs, and then, the top wing is placed on the vertical tail. The motor is placed on an upward projection from the bottom wing with proper alignment of the motor axis with the horizontal line parallel to CG. The components are placed approximately, so that the torque due to differential weight will help balance the counter-torque during flight. The autopilot needs to be placed on a vibration pad to reduce the effect of higher motor vibration.

6 Final configuration design

The final configuration is arrived at after evaluating the aerodynamic performance of the MAV during remote-controlled (RC) flight tests, structural integrity during the crash landing. The addition of a dihedral angle is the major modification performed to improve the lateral stability after flight

test observations. Dihedral is provided only on the top wing considering the ease in manufacturing, as having a dihedral on the lower wing does not allow ease of accommodating the components. A larger dihedral angle makes the MAV's spiral mode stable but Dutch roll mode unstable. A 12° dihedral on the top wing is provided considering this trade-off between and the stability of the two modes and also from the manufacturing perspective. Two halves of the top wing are attached separately to the vertical tail at a specified angle to provide dihedral on the top wing. The structural material used in different sections is shown in Fig. 11. Figure 12 shows the fabricated complete model of “Skylark”.

After the finalization of configuration, the mathematical model of the MAV is developed using CAD modelling, wind tunnel test, and standard empirical results. The nonlinear mathematical model is linearized at the various operating points to obtain the linear model, and stability and trim analysis are performed. The various operating points considered are three different flight conditions: (a) straight and level flight, (b) steady and turning flight (turn radius of 25 m), and (c) climb and turning flight (turn radius of 30 m and flight path angle of 15°); at different velocities of 8 m/s, 9 m/s, 10 m/s, 11 m/s, and 12 m/s. The properties of the different dynamic modes of the “Skylark” at the velocity of 10 m/s for straight and level flight 10 m/s are shown in Table 11. The eigenvalues associated with the short period modes are $-2.44 + i 24.80$ and $2.44 + i 24.80$, phugoid modes are $-0.85 + i 1.42$ and $0.85 - i 1.42$, and dutch roll modes are $-0.70 + i 13.04$ and $-0.70 - i 13.04$. In this case, roll subsidence and spiral mode cannot be distinguished separately; the eigenvalues associated with the coupled roll subsidence and spiral mode are $-1.47 + i 1.93$ and $-1.47 - i 1.3$. The properties of the other modes are found to be on the same scale as other MAVs like “Black Widow”, “KH2013A”. Based on the properties of dynamic modes at the operating points, “Skylark” is found to be dynamically stable. It is to be noted that static values of rolling moment coefficient (C_l) and yawing moment coefficient (C_n) are not zero as the sideslip angle (β) and aileron deflection (δ_a) at trim condition are not zero due

Fig. 11 Different components of MAV structure

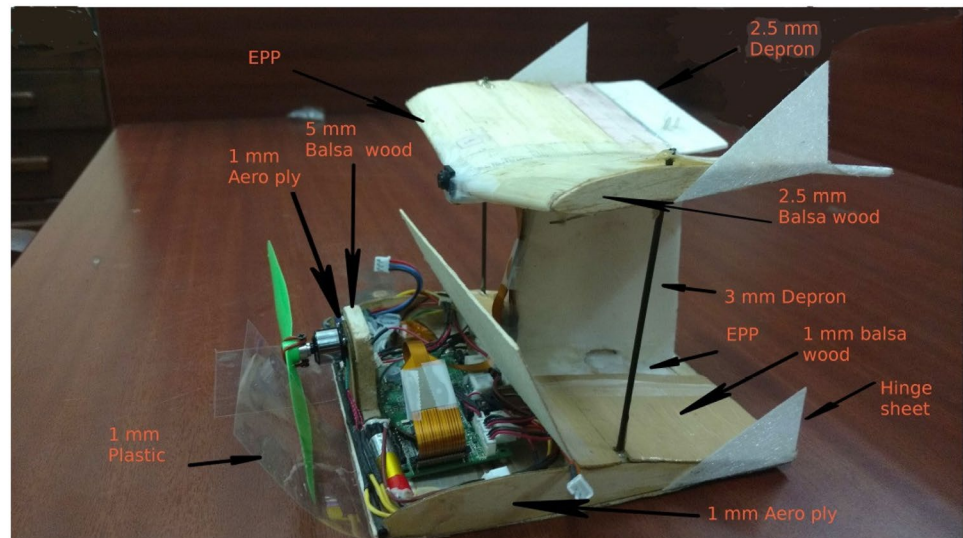


Fig. 12 Complete fabricated model

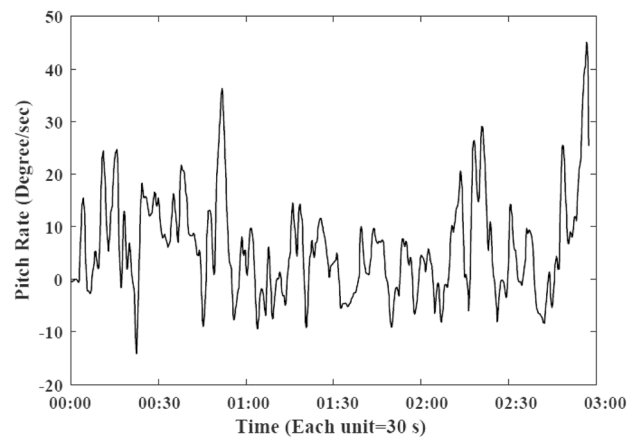


Fig. 13 Pitch rate

Table 11 Natural modes of “Skylark”

Parameter	Value
Short period mode frequency	24.80 rad/s
Short period mode damping ratio	0.097
Phugoid mode frequency	1.42 rad/s
Phugoid mode damping ratio	0.54
Dutch roll mode frequency	13.04 rad/s
Dutch roll mode damping ratio	0.05
Coupled roll subsidence and spiral mode frequency	1.93 rad/s
Coupled roll subsidence and spiral mode damping ratio	0.65

to propeller counter-torque. For straight and level flight of 10 m/s, the trim values of (β) and (δ_a) are -0.42^{circ} and 10.32^{circ} , and the values of (C_l) and (C_n) are 0.0027 and 0.0036.

The suitable estimator is designed for estimating the attitude angles, and estimation is validated through rate

table experiments. The basic controller is designed for the nominal performance of the plant, and an add-on advance controller is incorporated to handle the huge uncertainties involved in the MAV system dynamics. Different algorithms along with the autopilot software architecture are validated through Software in Loop Simulations (SILS) and Hardware in Loop Simulations (HILS). Finally, autonomous navigation is performed based on the waypoint following. For a typical flight, the body angular rates and Euler angles during a flight are shown in Fig. 13, 14, 15, 16, 17, and 18. Clearly, the angular states remain bounded during the flight.

The important design parameters observed from the flight tests are shown in Table 12. The endurance can be increased with the inclusion of a heavier battery as a part of the payload. Flight test videos of “Skylark” are available in this URL link.¹

¹ https://drive.google.com/file/d/1-65Sub-wucZfcE-_4DpO7Mr0iOr1OJiv/view?usp=sharing.

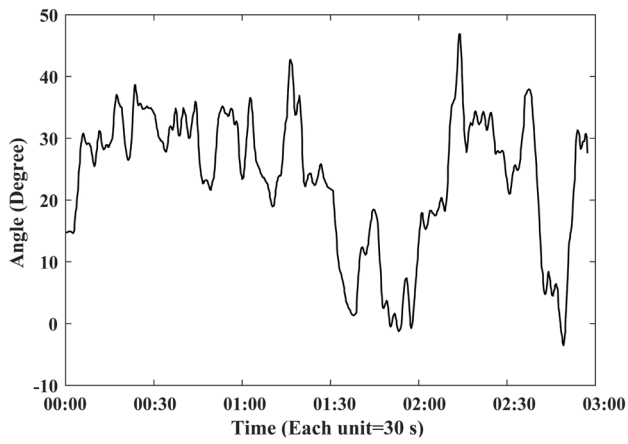


Fig. 14 Pitch angle

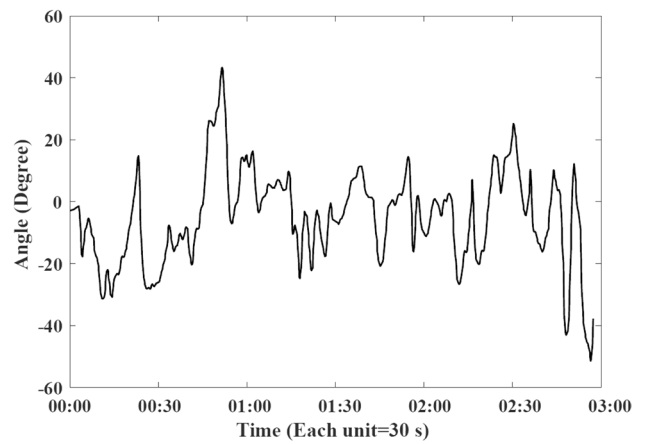


Fig. 17 Yaw rate

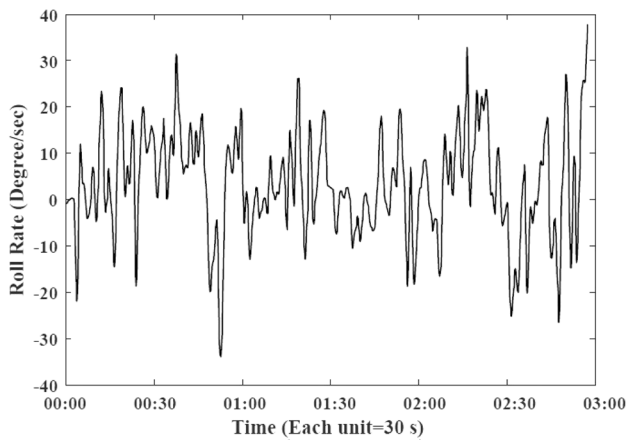


Fig. 15 Roll rate

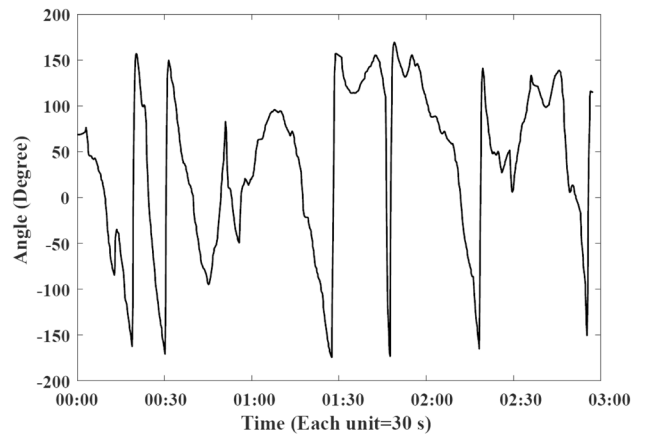


Fig. 18 Yaw angle

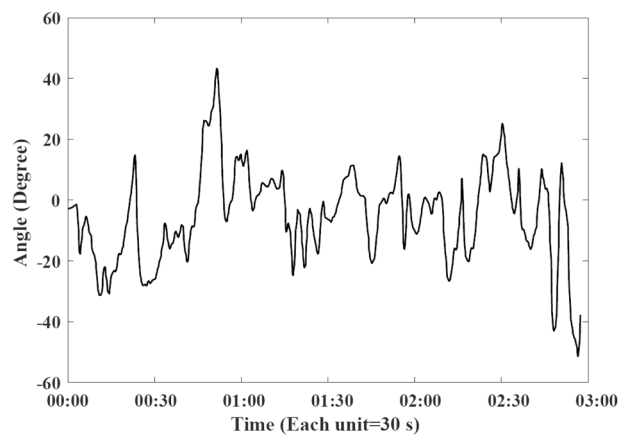


Fig. 16 Roll angle

Table 12 Final design summary

Parameter	Specification
Tested take-off weight	121 g
Tested payload	15 g
Maximum observed flight speed	11.5 m/s
Static margin	9 %
Minimum observed flight speed	7 m/s
Average endurance	7 min

7 Conclusions

This paper proposes a novel biplane MAV design to address the major challenges of high payload and poor static margin for a vision-assisted MAV system. In the proposed design, an optimum top wing is devised at the trailing edge, which offers a twofold advantage. The top wing acts as an additional lifting surface as it increases the payload-carrying capacity, and the placement of the wing toward the trailing edge has the effect of shifting the aerodynamic centre toward the trailing edge, which increases the static margin. The detailed design of different subsystems is performed considering the constraints of space, CG location, and strict weight and power budget. An integrated autopilot module is designed to include the image processing capabilities along with the conventional autopilot functionalities. The flying capability and the stability of the proposed design are validated through several flight tests. The designed MAV called “Skylark” has a wingspan of 150 mm, a chord of 140 mm, and a total take-off weight of 110 grams. The proposed design approach is expected to improve the capability, reliability, and efficiency of the MAV class of vehicles in unknown environments. Future work involves the real-time implementation of vision-based autonomous flight for the MAV class of vehicles. The main objective will be developing and implementing vision-based control, guidance, and estimation algorithms suitable for the MAV platform.

Supplementary Information The online version supplementary material available at <https://doi.org/10.1007/s13272-022-00570-w>.

Acknowledgements The authors would like to express their gratitude to Titas Bera, Shashank Shivkumar, Meghana Ramesh, Susheel Balasubramaniam, Eshaan Khanapuri, and Sidhant Dhall for their suggestions to the MAV design.

Declarations

Funding The work is funded under National Programme for Micro Air Vehicle (NP-MICAV) project of Defence Research Development Organization (DRDO). The authors would like to thank Aeronautics Research and Development Board (ARDB) for their funding and support for the project (Grant DARO/08102072/M/I/VE).

Conflict of interest The authors declare that they have no conflict of interest.

References

- McMichael, J.M., Francis, M.S.: Micro air vehicles-toward a new dimension in flight. DARPA document (1997)
- Grasmeyer, J., Keennon, M.: Development of the black widow micro air vehicle. In: 39th Aerospace Sciences Meeting and Exhibit, p. 127 (2001). <https://doi.org/10.2514/6.2001-127>
- Hwang, H., Chung, D., Yoon, K., Park, H., Lee, Y., Kang, T.: Design and flight test of a fixed wing mav. In: 1st UAV Conference, p. 3413 (2002). <https://doi.org/10.2514/6.2002-3413>
- Cosyn, P., Vierendeels, J.: Design of fixed wing micro air vehicles. *Aeronaut. J.* **111**(1119), 315–326 (2007). <https://doi.org/10.1017/S0001924000004565>
- Harikumar, K., Dhall, S., Bhat, M.S.: Nonlinear modeling and control of coupled dynamics of a fixed wing micro air vehicle. In: Control Conference (ICC), 2016 Indian, pp. 318–323. IEEE (2016). <https://doi.org/10.1109/INDIANCC.2016.7441153>
- Shyy, W., Lian, Y., Tang, J., Viieru, D., Liu, H.: Aerodynamics of low Reynolds number flyers. Cambridge: Cambridge University Press (2008). <https://doi.org/10.1017/CBO9780511551154>
- Wu, L., Ke, Y., Chen, B.M.: Systematic modeling of rotor-driving dynamics for small unmanned aerial vehicles. *Unmanned Syst.* **6**(02), 81–93 (2018)
- Burri, M., Bloesch, M., Taylor, Z., Siegwart, R., Nieto, J.: A framework for maximum likelihood parameter identification applied on mavs. *J. Field Robot.* **35**(1), 5–22 (2018)
- Thipyopas, C., Moschetta, J.M.: From development of micro air vehicle testing research to the prototype of tyto: low speed biplane mav. In: 26th AIAA Applied Aerodynamics Conference, p. 6250 (2008). <https://doi.org/10.2514/6.2008-6250>
- Zafirov, D., Panayotov, H.: Joined-wing test bed uav. *CEAS Aeronaut. J.* **6**(1), 137–147 (2015). <https://doi.org/10.1007/s13272-014-0134-z>
- Singh, S., Sahanpal, M., Narula, A., Kaur, J., Rao, Y., Amar, A.: Design and development of micro aerial vehicle. *Adv. Aerosp. Sci. Appl.* **4**, 91–98 (2014)
- Frediani, A., Rizzo, E., Cipolla, V., Chiavacci, L., Bottoni, C., Scanu, J., Iezzi, G.: Development of ulm prandtlplane aircraft and flight tests on scaled models. In: XIX AIDAA Congress, XIX Congresso Nazionale AIDAA, Milan, Italy (2007)
- Moschetta, J.M., Thipyopas, C.: Aerodynamic performance of a biplane micro air vehicle. *J. Aircr.* **44**(1), 291–299 (2007). <https://doi.org/10.2514/1.23286>
- Vogeltanz, T.: Conceptual design and control of twin-propeller tail-sitter mini-uav. *CEAS Aeronaut. J.* **10**(3), 937–954 (2019). <https://doi.org/10.1007/s13272-019-00388-z>
- Kellogg, J., Cylinder, D., Foch, R., Kahn, A., Ramamurti, R., Srull, D., Bovais, C., Gardner, J., Sandberg, W.: Development and testing of unconventional micro air vehicle configurations. In: 2nd AIAA Unmanned Unlimited Conf. and Workshop & Exhibit, p. 6656 (2003). <https://doi.org/10.2514/6.2003-6656>
- Nagel, A., Levy, D.E., Shepshelovich, M.: Conceptual aerodynamic evaluation of mini/micro uav. In: 44th AIAA Aerospace Sciences Meeting and Exhibit, p. 1261 (2006). <https://doi.org/10.2514/6.2006-1261>
- Hrishikeshavan, V., Bogdanowicz, C., Chopra, I.: Design, performance and testing of a quad rotor biplane micro air vehicle for multi role missions. *Int. J. Micro Air Veh.* **6**(3), 155–173 (2014). <https://doi.org/10.1260/1756-8293.6.3.155>
- Hassanalain, M., Abdelkefi, A.: Classifications, applications, and design challenges of drones: a review. *Prog. Aerosp. Sci.* **91**, 99–131 (2017). <https://doi.org/10.1016/j.paerosci.2017.04.003>
- Darvishpoor, S., Roshanian, J., Raissi, A., Hassanalain, M.: Configurations, flight mechanisms, and applications of unmanned aerial systems: a review. *Prog. Aerosp. Sci.* (2020). <https://doi.org/10.1016/j.paerosci.2020.100694>
- Suresh, C., Ramesh, K., Paramaguru, V.: Aerodynamic performance analysis of a non-planar c-wing using cfd. *Aerosp. Sci. Technol.* **40**, 56–61 (2015). <https://doi.org/10.1016/j.ast.2014.10.014>
- Sadraey, M.H.: Aircraft Design: A Systems Engineering Approach. Wiley, Hoboken (2012)

22. Rais-Rohani, M., Hicks, G.R.: Multidisciplinary design and prototype development of a micro air vehicle. *J. Aircr.* **36**(1), 227–234 (1999). <https://doi.org/10.2514/2.2429>
23. Bingaman, J.: Unmanned aircraft and the applicability of military flying qualities standards. In: *AIAA Atmospheric Flight Mechanics Conference*, pp. 4415–4439 (2012). <https://doi.org/10.2514/6.2012-4415>
24. Foster, T., Bowman, J.: Dynamic stability and handling qualities of small unmanned-aerial vehicles. In: *43rd AIAA Aerospace Sciences Meeting and Exhibit*, pp. 1023–1035 (2005). <https://doi.org/10.2514/6.2005-1023>
25. Holmberg, J., Leonard, J., King, D., Cotting, M.: Flying qualities specifications and design standards for unmanned air vehicles. In: *AIAA Atmospheric Flight Mechanics Conference and Exhibit*, pp. 6555–6569 (2008). <https://doi.org/10.2514/6.2008-6555>
26. anon: Department of defense interface standard, flying qualities of piloted airplanes. MIL-STD-1797B (2006)
27. Moorhouse, D., Woodcock, R.: US Military Specification mil-f-8785c. US Department of Defense, Arlington (1980)
28. Tennekes, H., Pennycuik, C.: The simple science of flight: from insects to jumbo jets. *Nature* **381**(6578), 126 (1996)
29. Maqsood, A., Chang, C., Go, T.: Experimental investigation of a biplane micro air vehicle. In: *28th Congress of the International Council of the Aeronautical Sciences* (2012)
30. Roedts, R.: Design of a biplane wing for small-scale aircraft. In: *47th AIAA Aerospace Sciences Meeting Including The New Horizons Forum and Aerospace Exposition*, p. 207 (2009). <https://doi.org/10.2514/6.2009-207>
31. Kang, H., Genco, N., Altman, A.: Empirically derived biplane lift as a function of gap and stagger. *J. Aircr.* **50**(1), 292–298 (2013). <https://doi.org/10.2514/1.C031111>
32. Kang, H., Genco, N., Altman, A.: Gap and stagger effects on biplanes with end plates: part i. In: *47th AIAA Aerospace Sciences Meeting Including The New Horizons Forum and Aerospace Exposition*, p. 1085 (2009). <https://doi.org/10.2514/6.2009-1085>
33. Moschetta, J.M., Thipyopas, C.: Optimization of a biplane micro air vehicle. In: *23rd AIAA Applied Aerodynamics Conference*, p. 4613 (2005). <https://doi.org/10.2514/6.2005-4613>
34. Kang, H., Bichal, A., Altman, A.: Aerodynamic effects of end plates on biplane wings. In: *46th AIAA Aerospace Sciences Meeting and Exhibit*, p. 317 (2008). <https://doi.org/10.2514/6.2008-317>
35. Thipyopas, C., Moschetta, J.M.: A fixed-wing biplane mav for low speed missions. *Int. J. Micro Air Veh.* **1**(1), 13–33 (2009). <https://doi.org/10.1260/1756-8293.1.1.13>
36. Anderson, J.D., Bowden, M.L.: *Introduction to flight*. New York: McGraw-Hill Higher Education (2005)
37. Shyy, W., Lian, Y., Tang, J., Viieru, D., Liu, H.: *Aerodynamics of Low Reynolds Number Flyers*, vol. 22. Cambridge University Press, Cambridge (2007). <https://doi.org/10.1017/CBO9780511551154>
38. Mueller, T.J.: Fixed and flapping wing aerodynamics for micro air vehicle applications. *Am. Inst. Aeronaut. Astronaut.* (2001). <https://doi.org/10.2514/4.866654>
39. Aboezez, A., Hassanalian, M., Desoki, A., Elhadidi, B., El-Bayoumi, G.: Design, experimental investigation, and nonlinear flight dynamics with atmospheric disturbances of a fixed-wing micro air vehicle. *Aerosp. Sci. Technol.* **97**, 105636 (2020). <https://doi.org/10.1016/j.ast.2019.105636>
40. Tsai, B.J., Fu, Y.C.: Design and aerodynamic analysis of a flapping-wing micro aerial vehicle. *Aerosp. Sci. Technol.* **13**, 383–392 (2009). <https://doi.org/10.1016/j.ast.2009.07.007>
41. Gabriel, E., Mueller, T.: Low-aspect-ratio wing aerodynamics at low Reynolds number. *AIAA J.* **42**(5), 865–873 (2004). <https://doi.org/10.2514/1.439>
42. Sudhakar, S., Chandankumar, A., Venkatakrisnan, L.: Influence of propeller slipstream on vortex flow field over a typical micro air vehicle. *Aeronaut. J.* **121**(1235), 95–113 (2017). <https://doi.org/10.1017/aer.2016.114>
43. Shams, T.A., Shah, S.I.A., Shahzad, A., Javed, A., Mehmod, K.: Experimental investigation of propeller induced flow on flying wing micro aerial vehicle for improved 6dof modeling. *IEEE Access* **8**, 179626–179647 (2020). <https://doi.org/10.1109/ACCESS.2020.3026005>
44. Harikumar, K., Pushpangathan, J.V., Sundaram, S.: Effects of propeller flow on the longitudinal and lateral dynamics and model couplings of a fixed-wing micro air vehicle. *Proc. Inst. Mech. Eng. Part G J. Aerosp. Eng.* (2020). <https://doi.org/10.1177/0954410020966155>
45. Null, W., Noscek, A., Shkarayev, S.: Effects of propulsive-induced flow on the aerodynamics of micro air vehicles. In: *23rd AIAA Applied Aerodynamics Conference*, p. 4616 (2005). <https://doi.org/10.2514/6.2005-4616>
46. Sperry, M.T., Wong, K.: Design and development of a micro air vehicle (μ av) concept: Project bidule. In: *The 9th Annual International Aerospace Congress*. School of Aerospace, Mechanical and Mechatronic Engineering, University of Sydney, NSW, Australia (2001)
47. Staples, G.: The details of electric radio controlled air-craft. <https://www.electricircraftguy.com/>. 2015. Accessed 1 Apr 2015